Supporting Information

1. Information of MAC solid-phase carrier

Table S1 Information of six MAC solid-phase carriers.

MAC type	BET surface area/$m^2 \cdot g^{-1}$	Mesopore ratio/%	Average pore radius/nm	Pore volume/$cc \cdot g^{-1}$	Manufacturers
MAC-1	346	27.6	4.83	0.29	Jiangsu Youhuada Purification Material Co., Ltd
MAC-2	366	29.1	5.65	0.31	
MAC-3	450	62.9	8.14	0.71	
MAC-4	537	76.5	12.77	0.83	Henan Zhongju Purification Materials Co., Ltd
MAC-5	1281	24.5	2.39	0.56	
MAC-6	1624	60.5	2.43	0.77	

2. Preparation and application of EPP-PDA@MAC electrode

The preparation of the EPP-PDA@MAC electrode involved several steps for uniform slurry synthesize and electrode assembly. Initially, EPP-PDA@MAC was mixed with conductive carbon black (VXC27, Cabot Corporation Co.) and polyvinylidene fluoride (Arkema Co.) in a mass ratio of 8:1:1, followed by the addition of 5 mL 1-methyl-2-pyrrolidone. This mixture was stirred in a magnetic stirrer for 6 h to form a uniform slurry. Subsequently, the slurry was evenly coated onto a titanium plate with an area of 5 cm*5 cm and dried at 80°C for 10 h, resulting in the formation of the EPP-PDA@MAC electrode. To assemble the capacitive deionization (CDI) device, a layer of cation exchange membrane was applied to the surface of the EPP-PDA@MAC electrode, while an anion exchange membrane was applied to the surface of another MAC electrode. These two electrodes, along with diaphragm gaskets and other necessary components, were assembled to form the CDI device. In the adsorption and desorption experimental setup, a peristaltic pump was utilized to uniformly pump gallium nitrate solution into the water inlet of the CDI device at a flow rate of 10 mL/min. The liquid in the outlet section was exported to the same beaker via a tube. An external DC constant voltage power supply was employed to power the

counter electrode, with the positive electrode connected to the MAC electrode and the negative electrode connected to the EPP-PDA@MAC electrode, initiating the adsorption. Ga^{3+} were fixed on the EPP-PDA@MAC electrode by electrostatic force during adsorption process. After that, the electrodes were reversed to initiate the desorption experiment, simultaneously triggering the pump to circulate deionized water. Consequently, Ga^{3+} were desorbed from the EPP-PDA@MAC electrode under the applied reversed electric field and then was carried away by the flowing deionized water.

3. Atherton-Todd reaction

Historically, the Atherton-Todd (AT) reaction has been employed to synthesize phosphoramidates using diakyl phosphite and primary amine in the presence of carbon tetrachloride and alkali. This reaction has been explored further by optimizing reaction conditions and expanding nucleophile options. Organophosphorus compounds commonly used in the A-T reaction can be classified into tetra- and penta-coordinated phosphides, depending on the coordination number of phosphorus atoms. Tetra-coordinated phosphines encompass *O, O*-dialkyl phosphonates (i), hypophosphonates (ii), and dialkyl phosphine oxides (ii), as shown in Fig. S1 [1]. While classical A-T reactions initially relied on amines or alcohols as primary nucleophiles, subsequent research have revealed the applicability of phenol as alternative nucleophiles [1, 2]. Carbon tetrachloride, traditionally used as the halogenating reagent, has been replaced with safer alternatives like sodium hypochlorite and copper chloride due to its carcinogenic nature [3, 4]. The general formula for the A-T reaction is depicted in Fig. S1.

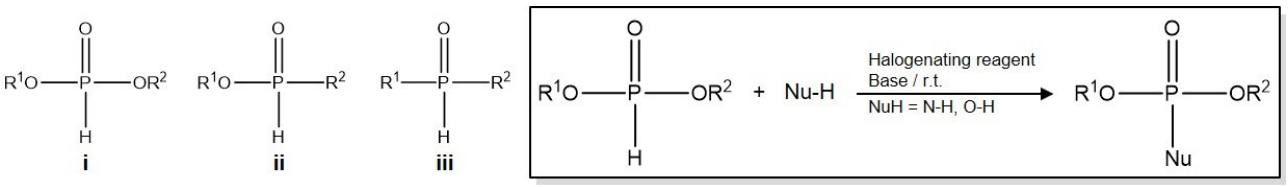

Fig. S1. Classification of tetra-coordinated phosphines and the Atherton-Todd reaction equation.

4. Parameter optimization of the P-PDA@MAC preparation

4.1. MAC particle size

MAC-6 was ground and sieved into various mesh size to synthesis six additional kinds of P-PDA@MAC. The BET characterization results (Table S2) confirmed that the grinding process resulted in

decreased BET specific surface, might leading to the reduced phosphoryl functional groups and lower adsorption efficiency of the P-PDA@MAC.

Table S2 The pore structure characterization results of MAC in different particle size.

Particle size/mesh	Specific surface area/$m^2 \cdot g^{-1}$			Pore volume/$cc \cdot g^{-1}$			Pore radius/nm	
	BET	BJH	Micropore	Total	BJH	Micropore	Single point	BJH
20-60	1765	265	2213	0.84	0.21	0.79	0.96	2.33
60-100	1684	310	2149	0.84	0.25	0.76	1	2.34
100-140	1497	258	1898	0.74	0.21	0.67	0.99	2.34
140-180	1484	262	1892	0.74	0.22	0.67	1	2.34
180-220	1465	260	1862	0.73	0.21	0.66	1	2.34
220-260	1398	280	1796	0.71	0.23	0.64	1.02	2.35

4.2. Dosage of DA

The thickness of the PDA layer can be controlled by adjusting the DA dosage, and the thinnest layer can reach about ~1 nm without great negative influence on the surface area and pore structure of carrier [5]. SEM characterization (Fig. S2) of the EPP-PDA@MAC fabricated with different DA dosages revealed distinct morphology changes. As the n_{DA} increased, the surface of EPP-PDA@MAC was initially loose and porous (0.03 mmol), then there is a uniform distribution of small particles signaling the formation of PDA layer (0.05-0.07 mmol) [6, 7], then the particle density and size increased (0.1 mmol) , finally the particles began to aggregate and form a thick layer (0.2-0.5 mmol). Therefore, when the DA dosage was 0.07 mmol, a thin and uniform PDA layer was formed, which enhanced the modification process and not affect the MAC structure. Higher DA dosage (≥0.07 mmol) led to dense PDA deposition, reducing effective surface area and binding sites for metal ions, thereby diminishing adsorption efficiency. Consequently, an optimal DA dosage of 0.07 mmol was selected to maximize adsorption capacity while preserving pore structure integrity.

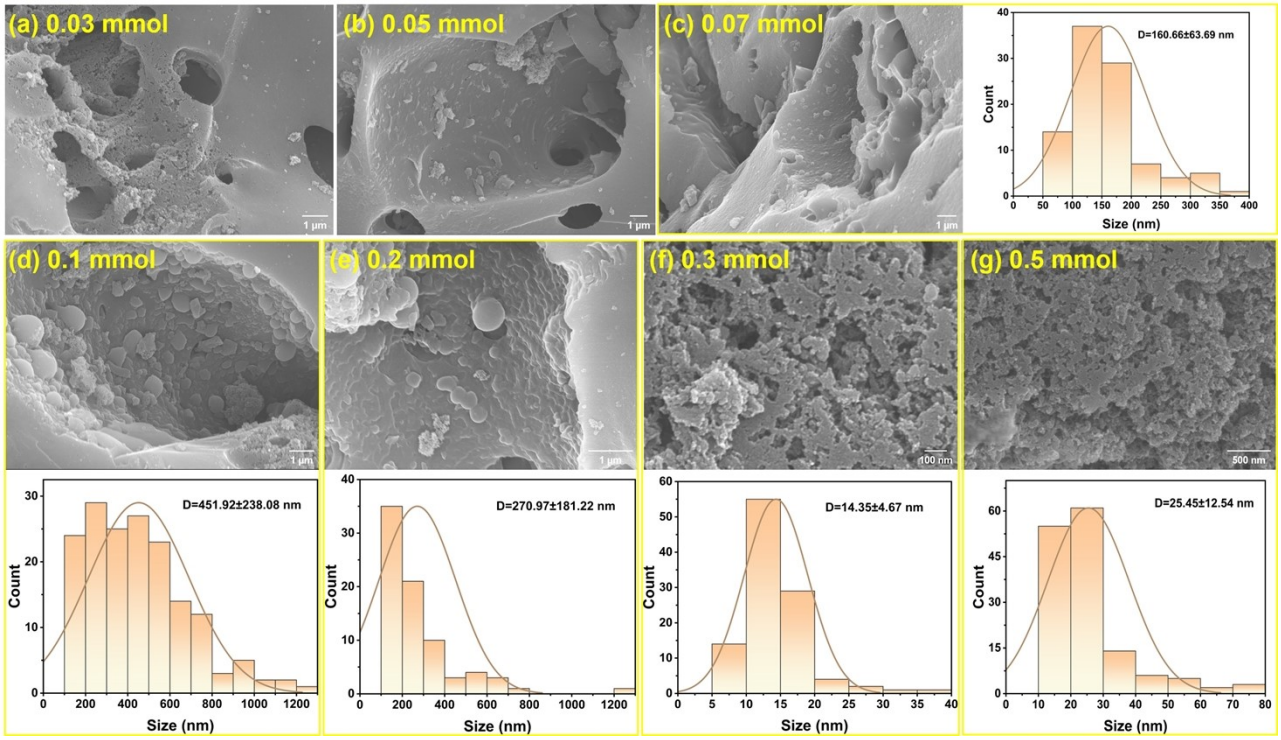

Fig. S2. Surface morphology changes of EPP-PDA@MAC and statistical analysis of particle size with increasing dopamine dosage: (a) n_{DA}=0.03 mmol, (b) n_{DA}=0.05 mmol, (c) n_{DA}=0.07 mmol, (d) n_{DA}=0.1 mmol, (e) n_{DA}=0.2 mmol, (f) n_{DA}=0.3 mmol, (g) n_{DA}=0.5 mmol.

4.3. Dosage of NaOH

The solution pH was adjusted to 7.3-12.0 by adjusting the NaOH dosage. Following a defined modification process, the endpoint pH of the liquid phase system was determined alongside the adsorption efficiencies of the prepared materials under different pH conditions. The significant increase in the endpoint pH compared to the initial pH was observed in Fig. 1e, indicating that the modification process consumed alkali coinciding with the PDA polymerization reaction and A-T reaction mechanism [8, 9]. Furthermore, the adsorption efficiencies showed a significant decrease with the increase of the initial pH and NaOH dosage. The reason might be the excessive oxidation of PDA, which was consistent with the continuous darkening of the solution color at the endpoint [6]. Therefore, optimizing NaOH dosage to 0.1 mL ensured an initial liquid-phase system pH of 7.3, yielding the adsorbent with optimal performance.

4.4. Temperature and time

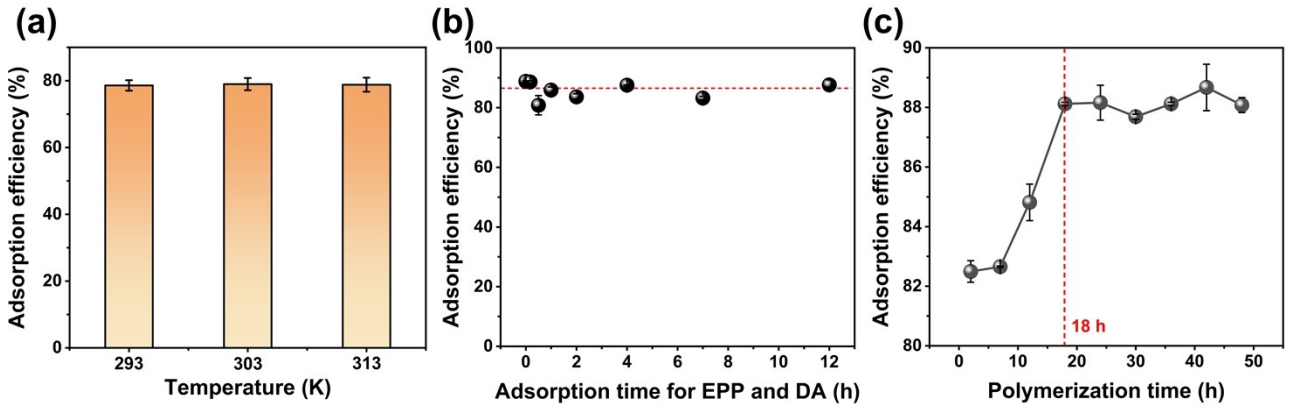

Fig. S3. Effect of (a) temperature, (b) precursor adsorption time, and (c) polymerization time on the adsorption efficiency of EPP-PDA@MAC.

4.5. BET characterization

The N_2 adsorption-desorption isotherm of EPP-PDA@MAC exhibited a significant upward trend with increasing pressure, accompanied by a pronounced hysteresis loop between the adsorption and desorption branches (Fig. S4a). This behavior is characteristic of IV isotherms, indicating the presence of abundant mesoporous structures within EPP-PDA@MAC.[10] Additionally, the pore size distribution analysis revealed a rich presence of micropores alongside a substantial quantity of mesopores, with mesopore diameters ranging from 2 to 5 nm (Fig. S4b). The BET specific surface area, pore volume, and pore diameter for EPP-PDA@MAC were summarized in Table S3.

Table S3 The pore structure characterization results of MAC and EPP-PDA@MAC.

Materials	**Specific surface area/$m^2 \cdot g^{-1}$**			**Pore volume/$cc \cdot g^{-1}$**			**Pore radius/nm**	
	BET	**BJH**	**Micropore**	**Total**	**BJH**	**Micropore**	**Single point**	**BJH**
MAC	1765	265	2213	0.84	0.21	0.79	0.96	2.33
EPP-PDA@MAC	1408	198	1759	0.67	0.16	0.63	0.95	2.34

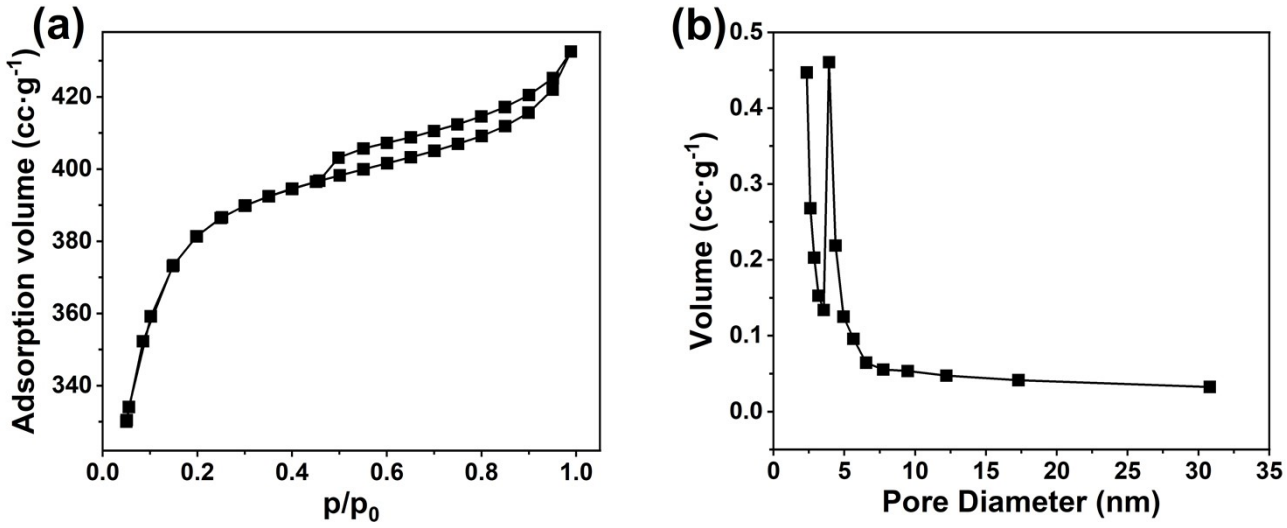

Fig. S4. (a) N_2 adsorption-desorption isotherm and (b) pore size distribution curves of EPP-PDA@MAC.

5. Adsorption and desorption performance of EPP-PDA@MAC

5.1. Effect of anion species

To elucidate the influence of the main anion species (sulfate ions, chloride ions, and nitrate ions) in the adsorption phase, solutions of $In(NO_3)_3$, $In_2(SO_4)_3$, $InCl_3$, $Ga(NO_3)_3$, $Ga_2(SO_4)_3$, and $GaCl_3$ with equivalent metal ion concentrations and pH were prepared. According to Fig. S5, the adsorption efficiencies of EPP-PDA@MAC for In^{3+} and Ga^{3+} were notably higher in nitrate ion-containing solutions compared to those containing sulfate or chloride ions. Therefore, subsequent experiments were performed using the NO_3^- medium.

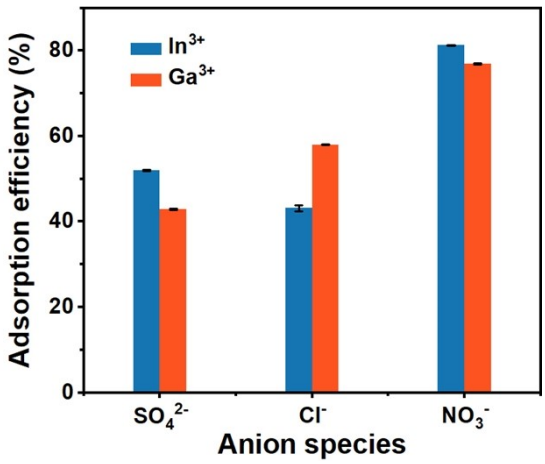

Fig. S5. Effect of major anion species on the adsorption efficiency of EPP-PDA@MAC.

5.2. Adsorption kinetic models fitting analysis

5.2.1 Adsorption kinetic models

(1) Pseudo-first-order model:

$$Q_t = Q_e \times \left(1 - e^{-k_1 t}\right) \tag{1}$$

Where Q_t and Q_e (mg·g^{-1}) were the adsorption capacity of ions at time t (min) and the final equilibrium; k_1 (min^{-1}) was the rate constant of the pseudo-first-order model.

(2) Pseudo-second-order model:

$$Q_t = \frac{k_2 \times Q_e^2 \times t}{1 + k_2 \times Q_e \times t} \tag{2}$$

Where Q_t and Q_e were the same as above; k_2 (min^{-1}) was the rate constant of the pseudo-second-order model.

(3) Elovich model:

$$Q_t = a + b \times ln \tag{3}$$

Where Q_t was the same as above; a and b were the adsorption kinetic rate constants of the Elovich model.

(4) Boyd's film-diffusion model:

$$F(t) = 1 - \left(\frac{6}{\pi^2}\right) \sum_{n=1}^{\infty} \left(\frac{1}{\pi^2}\right) exp(-n^2 \times B_t) \tag{4}$$

Where $F(t)$ was the fractional attainment of equilibrium, at different times t, and B_t was a function of $F(t)$:

$$F(t) = \frac{Q_t}{Q_e} \tag{5}$$

Where Q_t and Q_e were the same as above.

By applying the Fourier transform and then integration, Reichenberg managed to obtain the following approximations:

For $F(t)$ values > 0.85,

$$B_t = 0.4977 - ln(1 - F(t)) \tag{6}$$

And, for $F(t)$ values < 0.85,

$$B_t = [\sqrt{\pi} - \sqrt{\pi - (\frac{\pi^2 F(t)}{3})}]^2$$

(5) Bangham pore diffusion model:

$$log\left[log\left(\frac{C_0}{C_O - Q_t \times m}\right)\right] = log\left(\frac{K_0 \times m}{2.303 \times V}\right) + \alpha \times log\, t \quad (7)$$

Where, Q_t was the same as above; C_0 was the initial concentration of the adsorbate in solution (mg·L^{-1}); m was the weight of adsorbent (g·L^{-1}); V was the volume of solution (mL) and α (less than 1) and K_0 were the constants.

(6) Intra-particle diffusion model:

$$Q_t = k_s \times t^{0.5} + C \quad (8)$$

Where Q_t was the same as above; k_s (g·mg^{-1}·min$^{0.5}$) was the rate constant of the intra-particle diffusion model; C (mg·g^{-1}) was a constant revealing the number of boundary layers of the adsorbent. The smaller the C value, the fewer the impact of boundary layers on the intra-particle diffusion. The diffusion coefficients were calculated to determine the rate control step of the adsorption process:

$$\frac{Q_t}{Q_e} = 6(\frac{D_1}{\pi R^2})^{0.5} t^{0.5} \quad (9)$$

$$ln\left(1 - \frac{Q_t}{Q_e}\right) = ln\frac{6}{\pi^2} - (\frac{D_2 \pi^2}{r^2} t) \quad (10)$$

Where D_1 was the film diffusion coefficient; D_2 was the intra-particle diffusion coefficient; r was the radius of the adsorbent. If the adsorption rate was controlled by film diffusion, the value of D_1 was between 10^{-6}-10^{-11} cm^2/s. And if the adsorption rate was controlled by pore diffusion, the value of D_2 was between 10^{-11}-10^{-13} cm^2/s.

5.2.2 Results and analysis

According to Fig. 3c, Fig. S6, and Table S4, the regression coefficients of the Elovich model (R^2> 0.96) were the highest compared to other models. In addition, good fits were also observed with the Pseudo-second-order model (R^2 > 0.94) and Boyd's film diffusion model (R^2 > 0.95), indicating the influence of chemical reaction for adsorption and film diffusion as one of the rate-limiting steps during adsorption process.

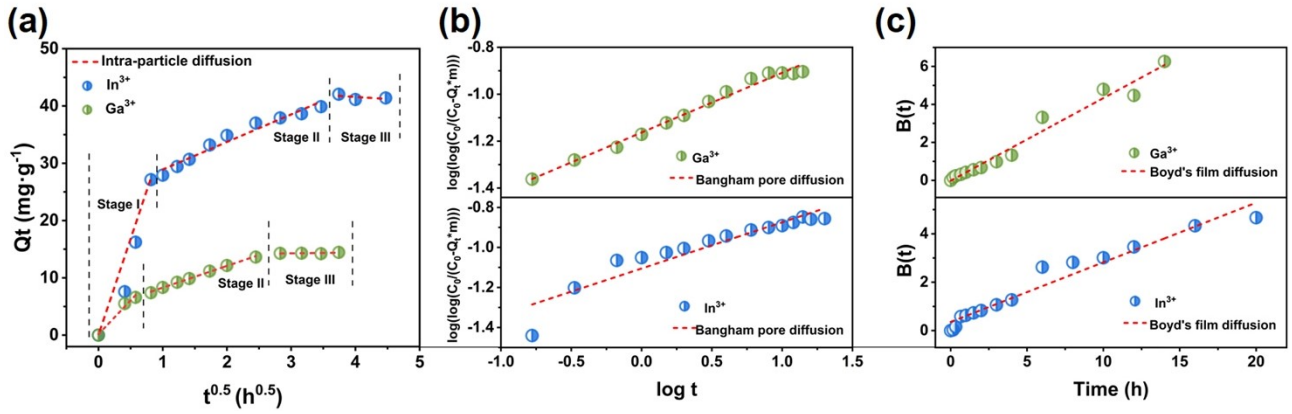

Fig. S6. Kineties fitting models of In^{3+} and Ga^{3+} adsorption on EPP-PDA@MAC. (a) Intra-particle diffusion model, (b) Bangham pore diffusion model, and (c) Boyd's film diffusion model.

Table S4 Correlation coefficients of six kinetics models for In^{3+} and Ga^{3+} adsorption.

Models		**R^2**	
		In^{3+}	**Ga^{3+}**
Pseudo-first-order model		0.8903	0.8411
Pseudo-second-order model		0.9796	0.9417
Elovich model		0.9583	0.9883
Boyd's film diffusion model		0.9534	0.9704
Bangham pore diffusion model		0.8806	0.9861
Intra-particle diffusion model	Stage I	0.9411	0.9817
	Stage II	0.9614	0.9970
	Stage III	0.8869	0.9880

5.3. Adsorption isotherm models fitting analysis

5.3.1. Adsorption isotherm models

(1) Langmuir model:

$$Q_e = \frac{Q_m b C_e}{1 + b C_e} \tag{11}$$

Where Q_e and C_e were the same as above; Q_m was the maximum adsorbed value of metal ion on the adsorbate; b was the Langmuir adsorption constant related to the binding energy.

(2) Freundlich model:

$$\log Q_e = \log K_f + \frac{1}{n} \log C_e \tag{12}$$

By plotting log versus $\log Q_e$, the constant K_f and the exponent $1/n$ could be calculated.

5.3.2 Fitting results

Table S5 Correlation coefficients of the Freundlich and Langmuir isotherm models for In^{3+} and Ga^{3+} adsorption.

Models	**Temperature/K**	**Parameters**	**Values**	
			In^{3+}	**Ga^{3+}**
Freundlich	298	R^2	0.967	0.982
	308	R^2	0.987	0.984
	318	R^2	0.971	0.980
Langmuir	298	K_L ($L \cdot mg^{-1}$)	0.026	0.021
		R_L	0.1-0.9	0.4-0.9
		Q_m ($mg \cdot g^{-1}$)	125.1	140.7
		R^2	0.994	0.996
	308	K_L ($L \cdot mg^{-1}$)	0.021	0.017
		R_L	0.2-0.9	0.5-0.9
		Q_m ($mg \cdot g^{-1}$)	154.9	176.3
		R^2	0.996	0.996
	318	K_L ($L \cdot mg^{-1}$)	0.020	0.014

	R_L	0.2-0.9	0.5-0.9
	Q_m (mg·g^{-1})	188.4	243.7
	R^2	0.994	0.993

6. Comparison of EPP-PDA@MAC with other adsorbents

Table S6 Comparison of preparation parameters, adsorption ability and desorption conditions of different adsorbents for In^{3+} and Ga^{3+} in existing studies.

Adsorbents	Preparation parameters			Adsorption ability	
	Method	Condition	Toxic/ organic reagent	$Q_{m\text{-}In}$/ mg·g^{-1}	SF_{In}^{X}
PA-HPEI-OACF	Three steps: oxidation; hydrothermal reaction; mix and heat	60℃, 4 h; 140℃, 14 h (high pressure);80℃, 4 h	HNO_3, H_2SO_4, phytic acid,	34.2	798.8
SiO_2@GO-PO_3H_2	Four steps: mix, reflux and stir; water-bath	60℃, 4 h; 140℃, 14 h (high pressure); 80℃, 4 h	HCl, toluene, ethanol, DMF	149.9	23.2
Silica gel/GO IIC	Six steps: mix, stir and reflux; water-bath; acid leach	60℃, 4 h; 140℃, 14 h (high pressure); 80℃, 4 h	HCl, toluene, ethanol, DMF, tetrahydrofuran, maleic anhydride, methanol, AIBN, H_2SO_4	147.1	35.3
IRA-900 Resin	Three steps: mix and stir	80℃, 6 h; 25℃, 2 h (N_2 atmosphere); 25℃, 12 h	tetrahydrofuran, methanol	95.6	6.9
D2EHPA@Resin	One step: mix and stir	25℃, 2h	HCl, methanol, ethanol	/	/
CNT/UiO-66-NH_2	Three steps: mix and shake; hydrothermal reaction	ultrasound; 120℃, 24 h (high pressure); 100℃, 12 h (high pressure)	DMF, ethanol	/	/
Functionalized cellulose	Two steps: mix and reflux; ice bath and stir	25℃, 4 h; 0℃, N_2 atmosphere; 20℃, 5 h	thionyl chloride, DMF, ethanol	/	/
UiO-66-NH_2-membranes	Three steps: hydrothermal reaction; mix and stir; electrospinning	120℃, 24 h; 70℃, 24 h; ultrasound, 12 h; 15 kV	HCl, DMF, methanol, ethanol, tetrahydrofuran	/	/
TBP@SIO_2-P	Two steps: mix, rotary evaporation	25℃, 1 h; 40℃, 1 h	dichloromethane	/	/
Functional hydrogel	Two steps: mix, heat and stir; radiation	40℃, 500 rpm; 2 kGy radiation from 60Co-gamma source	acrylamide, AMPS	17.7	/
Tannic acid- cellulose	Three steps: radiation; water-bath; mix and stir	cooling of dry-ice, 30 kGy radiation from EB accelerator; 50℃, 2 h; 80℃, 24 h	None	35.6	/
P507@MAC	One step: mix and rotary evaporation	25℃, 10 min	dichloromethane	53.6	121.5
EPP-PDA@MAC	**One step: mix and shake**	**25℃, 18 h**	**None**	**125.1**	**382.4**

Adsorbents	Adsorption ability			Desorption conditions			Ref.
	$Q_{m\text{-}Ga}$/ mg·g^{-1}	SF_{Ga}^{X}	Cycle number; efficiency	Acid type	Concentration; ration; time	Efficiency	
PA-HPEI-OACF	/	/	3; 74%	HCl	0.1 mol·L^{-1}; 1.25 L·g^{-1}; /	90%	[11]
SiO_2@GO-PO_3H_2	/	/	10; 97% (fixed-bed)	H_2SO_4	1 mol·L^{-1}; 0.25 mL·min^{-1} (fixed-bed)	98%	[12]
Silica gel/GO IIC	/	/	5; 94% (fixed-bed)	H_2SO_4	2 mol·L^{-1}; 0.25 mL·min^{-1} (fixed-bed)	/	[13]
IRA-900 Resin	/	/	5; 73%	HCl	2 mol·L^{-1}; 0.1 L·g^{-1}; 2 h	82%	[14]
D2EHPA@Resin	28.1	/	3:90%	HCl	1 mol·L^{-1}; 0.1 L·g^{-1}; 2 h	85%	[15]
CNT/UiO-66-NH_2	25.0	3.9	5; 85%	HCl	1 mol·L^{-1}; 2.5 L·g^{-1}; /	95%	[16]
Functionalized cellulose	31.5	5.0	4; 50%	HCl	3 mol·L^{-1}; /; /	78%	[17]
UiO-66-NH_2-membranes	96.2	3.1	9;80%	HCl	1 mol·L^{-1}; /; /	90%	[18]
TBP@SIO_2-P	22.0	3478	/	HCl	8 mol·L^{-1}; 0.05 L·g^{-1}; 0.5 h	96%	[19]
Functional hydrogel	11.6	/	/	HNO_3	0.5 mol·L^{-1}; 5 L·g^{-1}; 12 h	80%	[20]
Tannic acid- cellulose	26.6	/	/	HCl	5 mol·L^{-1}; /; /	78%	[21]
P507@MAC	67.0	122.0	6; 93%	HNO_3	0.5 mol·L^{-1} (Ga^{3+}), 4 mol·L^{-1} (In^{3+}); 0.67 L·g^{-1}; 3 h	93% (Ga^{3+}), 91.5% (In^{3+})	Former work [22]
EPP-PDA@MAC	**140.7**	**239.0**	**9; 90% (Ga^{3+}), 85% (In^{3+})**	**HNO_3**	**0.5 mol·L^{-1} (Ga^{3+}), 2 mol·L^{-1} (In^{3+}); 0.67 L·g^{-1}; 3 h**	**92% (Ga^{3+}), 91% (In^{3+})**	**This work**

7. Comparison between EPP-PDA@MAC and commercial adsorbent P507@Resin

7.1. Adsorption ability of P507@Resin

According to Fig. S7, P507@Resin could selectively adsorb In^{3+} and Ga^{3+} from mix solutions. The maximum separation factors for In^{3+} and Ga^{3+} were 118 and 52 when the solution pH=0.5 and 2, respectively. At this point, the adsorption efficiency for In^{3+} and Ga^{3+} were 50% and 72%, respectively.

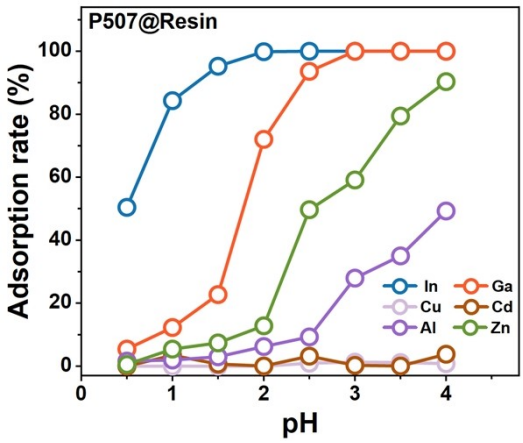

Fig. S7. Adsorption efficiency of P507@Resin for different metal ions in mix solution.

7.2. Green metrics calculation

The preparation methods for EPP-PDA@MAC and P507@Resin both follow a facile one step method (Fig. S8). The preparation method and parameters for EPP-PDA@MAC are detailed in Section 2.2. The synthetic method and parameters for P507@Resin are as follows: first, 10 mL of dichloromethane is used to wash the XAD-2 resin to remove impurities. Next, 0.3 mL of P507 is added to 20 mL dichloromethane to ensure the effective dispersion of the P507. Then, 0.2 g of the cleaned XAD-2 resin is introduced into the P507 and dichloromethane solution, and the mixture is subjected to rotary evaporation at 60°C for 1 h to eliminate the dichloromethane and achieve uniform impregnation of P507 into resin. Finally, the resulting solid product is dried at 393 K for 6 h to obtain P507@Resin. Due to the high viscosity of the P507, 10 g of water usually is required for cleaning the equipment during the whole process, which is particularly necessary when considering

scaling up production.

Synthetic method:

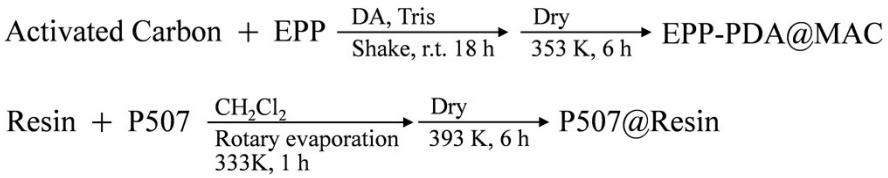

Fig. S8. Synthetic methods of EPP-PDA@MAC and P507@Resin.

The calculation of green metrics for both adsorbents is based on the mass of input and product. The following formulae were used for calculating reaction mass efficiency (RME), process mass intensity (PMI), mass productivity (MP), environmental impact factor (E), solvent and water Intensity (SI and WI).

$$\mathrm{RME} = \frac{\text{Mass of isolated product}}{\text{Total mass of reactants}} \times 100\% \quad (13)$$

$$\mathrm{MI} = \frac{\text{Total mass of input material in a process o}}{\text{Mass of product}} \quad (14)$$

$$\mathrm{PMI} = \frac{\text{Total mass of input material in the whole}}{\text{Mass of product}} \quad (15)$$

$$\mathrm{MP} = \frac{1}{\mathrm{PMI}} \times 100\% \quad (16)$$

$$\mathrm{E} = \mathrm{PMI} - 1 \quad (17)$$

$$\mathrm{SI} = \frac{\text{Total mass of solvents excl. water in the } wl}{\text{Mass of product}} \quad (18)$$

$$\mathrm{WI} = \frac{\text{Total mass of water used in the whole proc}}{\text{Mass of product}} \quad (19)$$

7.3. Calculation of production costs

To calculate the production costs of the adsorbent (100 kg), the quantities of chemical reagents,

the specifications and power of equipment were determined. Price of raw materials and the total reagent cost were obtained through consultations with major chemical reagent suppliers. Additionally, electricity costs were calculated based on the equipment' power consumption. Projected labor costs and equipment usage costs were incorporated to derive the unit production cost of these two adsorbents. All price and cost are expressed in Chinese yuan. Detailed information can be found in Table S7-8.

Table S7 Production cost analysis of EPP-PDA@MAC on industrial scale (100 kg)

Raw material cost (l00 kg adsorbent)	**Reagent**	**Mass /kg**	**Price /RMB·kg^{-1}**	**Manufacturer**	**Reagent cost /RMB**	**Total /RMB**
	Activated carbon	83	5	Zhongju Purification Materials Co	415	14015
	DA	6	1900	Bozhou Hongqi Pharmaceutical Co.	11400	
	Tris	3	65	Hubei New Desheng Material Technology Co.	195	
	EPP	71	28	Wuhan Canos Technology Co.	1988	
	Water	8333	0.002		17	
Electricity cost (l00 kg adsorbent)	**Equipment**	**Power /kW**	**Operating time/h**	**Consumption/ kW·h**	**Electricity cost /RMB**	**Total /RMB**
	High-capacity shaker	0.25	90	22.5	14	23
	Large oven	2.5	6	15	9	
Labor cost (l00 kg adsorbent)/RMB				400		
Equipment usage cost (l00 kg adsorbent)/RMB				200		
Unit production cost (l kg adsorbent)/RMB				146		

Table S8 Production cost analysis of P507@Resin on industrial scale (100 kg)

Raw material cost (l00 kg adsorbent)	**Reagent**	**Mass /kg**	**Price /RMB·kg^{-1}**	**Manufacturer**	**Reagent cost /RMB**	**Total /RMB**
	XAD-2	91	445	Jining Tongyi	40495	158734

	Resin			Chemical Co.		
	P507	91	550	Jining Tongyi Chemical Co.	50050	
	CH_2Cl_2	13636	5	Hefeng New Energy Co.	68180	
	Water	4545	0.002		9	
Electricity cost (l00 kg adsorbent)	**Equipment**	**Power /kW**	**Operating time/h**	**Consumption/ kW·h**	**Electricity cost/RMB**	**Total /RMB**
	large rotary evaporator	6.5	40	260	156	165
	large oven	2.5	6	15	9	
Labor cost (l00 kg adsorbent)/RMB				600		
Equipment usage cost (l00 kg adsorbent)/RMB				300		
Unit production cost (l kg adsorbent)/RMB				1598		

Note: According to the quotation from Jining Tangyi Chemical Co., the commercial price of P507@Resin is 1575 RMB/kg.

8. ^{1}H NMR spectrum of EPP-PDA

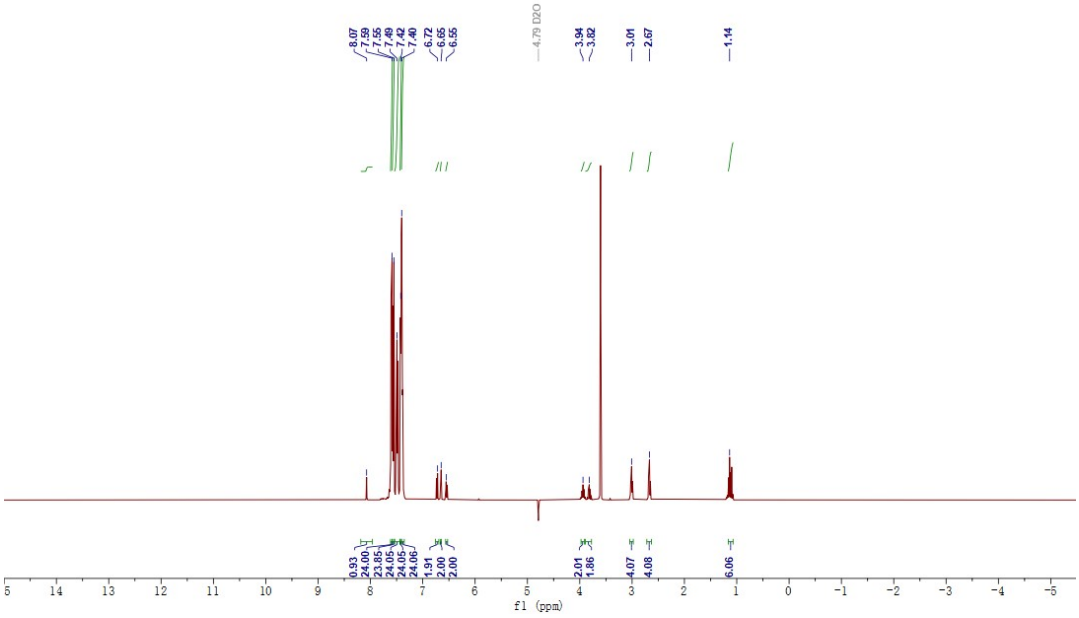

Fig. S9. ^{1}H NMR (400 MHz, Deuterium Oxide) spectrum of EPP-PDA: δ 8.07 (s, 1H), 7.59 (s, 24H), 7.55 (s, 24H), 7.49 (s, 24H), 7.42 (s, 24H), 7.40 (s, 24H), 6.72 (s, 2H), 6.65 (s, 2H), 6.55 (s, 2H), 3.94 (s, 2H), 3.82 (s, 2H), 3.01 (s, 4H), 2.67 (s, 4H), 1.14 (s, 6H). The peaks of D_2O and water are not marked, corresponding to 4.79 ppm.

9. Reusability test of the composite adsorbent (P507@MAC) via impregnation method

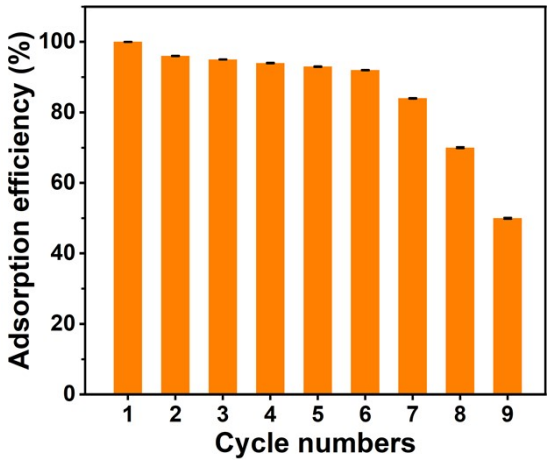

Fig. S10. Adsorption-desorption cycles of composite adsorbent (P507@MAC) via impregnation method for Ga^{3+}.

References

1. S. S. Le Corre, M. Berchel, H. Couthon-Gourves, J. P. Haelters and P. A. Jaffres, *Beilstein J Org Chem*, 2014, **10**, 1166-1196.
2. S. Cao, Y. Guo, J. Wang, L. Qi, P. Gao, H. Zhao and Y. Zhao, *Tetrahedron Letters*, 2012, **53**, 6302-6305.
3. J. C. Zhang, S. X. Cao, X. L. Yang and Y. F. Zhao, *Chinese Chemical Letters*, 2004, **15**, 646-648.
4. Y. B. Zhou, G. Wang, Y. Saga, R. W. Shen, M. Goto, Y. F. Zhao and L. B. Han, *Journal of Organic Chemistry*, 2010, **75**, 7924-7927.
5. K. H. Lim, H. Kweon and H. Kim, *Journal of The Electrochemical Society*, 2017, **164**, A1595-A1600.
6. Y. Duan, G. Dong, R. Wu, X. Zhao, M. Li, F. Zhang, Z. Song and H. Hao, *Polymer Engineering & Science*, 2022, **62**, 3390-3399.
7. M. Zhang, H. Zhang, F. Li, L. Yao, W. Peng and J. Zhang, *Catalysis Science & Technology*, 2022, **12**, 4255-4265.
8. Y. Y. Zhu, Y. Niu, Y. N. Niu and S. D. Yang, *Org Biomol Chem*, 2021, **19**, 10296-10313.
9. H. Feng, X. Zhu, R. Chen, Q. Liao, J. Liu and L. Li, *Chemical Engineering Journal*, 2016, **306**, 1017-1025.
10. L. Zou, L. Li, H. Song and G. Morris, *Water Res*, 2008, **42**, 2340-2348.
11. X. Gao, Z. Cao, C. Li, J. Liu, X. Liu and L. Guo, *New Journal of Chemistry*, 2022, **46**, 18952-18960.
12. M. Li, X. Meng, K. Huang, J. Feng and S. Jiang, *Hydrometallurgy*, 2019, **186**, 73-82.
13. M. Li, S. Tang, R. Liu, X. Meng, J. Feng, L. Zhou and Y. Chen, *Chemical Engineering Research and Design*, 2021, **168**, 135-145.
14. C. He, Y. Yang, M. Qi, Y. Jiang, Y. Wei, T. Fujita, G. Wang, S. Ma and W. Yang, *Journal of Environmental Chemical Engineering*, 2023, **11**.
15. J.-H. Chen, Y.-H. Chang, K.-C. Hsu and J.-C. Lin, *Chemical Engineering & Technology*, 2021, **44**, 2257-2268.
16. W. Li, C. Zhou, C. Li, W. Zhu, J. Shi and G. Liu, *Separation and Purification Technology*, 2023, **323**.
17. P. Raj, M. Patel and A. K. Karamalidis, *Separation and Purification Technology*, 2023, **323**.
18. M. Zhang, Q. Sun, Y. Wang, W. Shan, Z. Lou and Y. Xiong, *Chemical Engineering Journal*, 2021, **421**.
19. J. J. Meng, C. L. He, J. Zhou, T. Fujita, S. Y. Ning and Y. Z. Wei, *Journal of Applied Polymer Science*, 2020, **138**.
20. M. M. Bhuyan, O. B. Adala, H. Okabe, Y. Hidaka and K. Hara, *Journal of Environmental Chemical Engineering*, 2019, **7**.
21. J. Du, M. Zhang, Z. Dong, X. Yang and L. Zhao, *Separation and Purification Technology*, 2022, **286**.
22. W. Wang, X. Xu, D. Lai, Q. Xu, J. Li and Y. Wang, *Separation and Purification Technology*, 2024, **330**.